Anisotropic optical spin Hall effect in semiconductor microcavities

A. Amo,[1] T. C. H. Liew,[2] C. Adrados,[1] E. Giacobino,[1] A. V. Kavokin,[3,4] and A. Bramati[1]
[1]*Laboratoire Kastler Brossel, Ecole Normale Supérieure et CNRS, Université Pierre et Marie Curie, UPMC Case 74, 4 Place Jussieu, 75252 Paris Cedex 05, France*
[2]*Centre for Quantum Technologies, National University of Singapore, Singapore 117543, Singapore*
[3]*School of Physics and Astronomy, University of Southampton, Highfield, Southampton SO17 1BJ, United Kingdom*
[4]*Marie-Curie Chair of Excellence "Polariton devices," University of Rome II, via della Ricerca Scientifica 1, Rome 00133, Italy*
(Received 12 September 2009; published 23 October 2009)

Propagating, directionally dependent, polarized spin currents are created in an anisotropic planar semiconductor microcavity, via Rayleigh scattering of optically injected polaritons in the optical spin Hall regime. The influence of anisotropy results in suppression or enhancement of the pseudospin precession of polaritons scattered in specific directions. This is exploited to create intense spin currents by excitation on top of localized defects. A theoretical model considering the influence of the total effective magnetic field on the polariton pseudospin quantitatively reproduces the experimental observations.

DOI: 10.1103/PhysRevB.80.165325 PACS number(s): 78.67.De, 72.25.Dc, 71.36.+c, 72.25.Fe

I. INTRODUCTION

The field of spintronics has come a long way since the study of magnetic-dependent electron transport[1,2] and magnetic injection of electron spins[3] that began in the 1970s. The spin of an ensemble of particles, such as electrons, can encode a bit of information and today this is exploited to produce nonvolatile memory elements with high read/write speeds, high density, and low power consumption.[4,5]

Semiconductors have the potential for lower operating power and smaller size than their metallic counterparts and semiconductor spintronics[6] has been developing in parallel with metallic spintronics. However, while spin injection can be achieved in metallic systems by passing current through a ferromagnet, injection across a metal-semiconductor interface can be difficult due to the large impedance mismatch between the materials (although significant developments have been achieved).[7–9] An alternative method for the creation of spin currents in semiconductors is provided by the spin Hall effect (SHE),[10–13] which leads to a separation of spin-up and spin-down polarized electrons in both real and momentum space.[14] Despite the long spin coherence times of electrons in semiconductors[15] compared to those in (nonmagnetic) metals, the use of electrons as spin carriers still results in rapid dephasing and decay due to strong electron-electron scattering.

Recently, spin currents were generated in a different system, a semiconductor microcavity, using the so-called optical SHE (OSHE).[16] This optical analog of the SHE creates separated spin currents of polaritons in real and momentum space that travel a distance on the order of 100 μm, evidencing the realistic potential applications of polariton spin on the implementation of integrated polarization-based optical gates.[17,18] In this paper we show that we can use anisotropic fields to efficiently generate such spin currents in a preferred direction at engineered points of the sample.

Semiconductor microcavities are planar nanostructures designed to strongly couple light and matter: a pair of highly reflective mirrors confines cavity photons which are resonant with the exciton of a quantum well (QW) embedded in the cavity. The normal modes of such a system are exciton polaritons, neutral particles formed from the superposition of excitons and photons,[19] which do not suffer from the fast dephasing experienced by electrons.

The OSHE originates from the combined influence of the polarization splitting of transverse electric and transverse magnetic optical modes of the cavity (TE-TM splitting), and the elastic scattering of polaritons, excited by an optical pump, with disorder (Rayleigh scattering).[20] The combined effect of the long-range part of the exciton exchange interaction[21] and the TE-TM energy splitting of the optical modes[22] gives rise to the longitudinal transverse splitting (Δ_{LT}) of polaritons. In other words, Δ_{LT} originates from the dependence of the polariton energy on the angle between the polariton momentum $\mathbf{k}$ and its dipole oscillation direction, fixed by the plane of polarization of the linearly polarized excitation. Δ_{LT} depends on the magnitude of the in-plane wave vector $|\mathbf{k}|$, as illustrated in Fig. 1. In the OSHE configuration all polaritons are excited with the same $|\mathbf{k}|$ and this dependence can be disregarded.

The role of the Rayleigh scattering is to generate a system of polaritons with a plethora of different momentum directions after being pumped with a given $\mathbf{k}$. In a generalized form, the effect of Δ_{LT} on the polarization of exciton polaritons can be conveniently described within the pseudospin formalism by the introduction of an effective magnetic field, $\mathbf{\Omega}_{LT}$, whose orientation depends on the direction of the polariton wave vector while its magnitude is given by the modulus of $\mathbf{k}$.[20] The pseudospin itself depicts the polariton polarization state while the effective field is an optical analog of the Rashba field acting upon electron spins in semiconductor crystals lacking inversion symmetry.[23] The effective field $\mathbf{\Omega}_{LT}$ results in a $\mathbf{k}$-dependent precession of the polariton pseudospin, whose sign and magnitude depends on $\mathbf{k}$, leading to the separation of spin-up and spin-down polarized polaritons traveling in different directions in the Rayleigh ring (the ring of constant $|\mathbf{k}|$ created by Rayleigh scattering).[16]

In realistic microcavities, the Δ_{LT} splitting competes with the polarization splitting generated by the in-plane anisotropy of the sample. Even though molecular-beam epitaxy

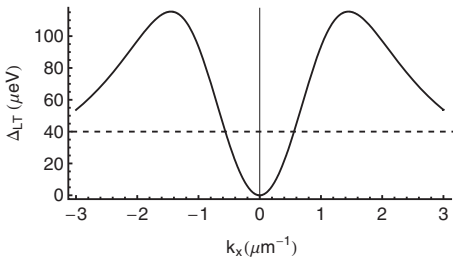

FIG. 1. Typical dependence of Δ_{LT} on $\mathbf{k}_x$. The dashed line represents the value of Δ_{LT} for our experimental conditions.

results in high-quality interfaces in semiconductor heterostructures, during the growth process of the QWs in the cavity, monolayer fluctuation islands and regions appear at each interface,[24] giving rise to asymmetric QWs in the growth direction. This asymmetry, for instance, has been shown to result in a carrier spin splitting at $k \neq 0$ due to the absence of inversion symmetry.[25–27] If the fluctuation islands are mainly oriented along a particular direction (for instance, given by the crystallographic axis) a linear-polarization splitting would arise even at $k=0$ due to the breakdown of the in-plane symmetry.[28] Additionally, in semiconductor microcavities the high number of accumulated layers of different materials in the Bragg mirrors gives rise to cross-hatched disorder originating from strain,[29] which may result in a constant splitting between the two linearly polarized components independent of the polariton momentum.

Effectively, anisotropy results in the appearance of a wave-vector independent linear-polarization splitting equivalent to a supplementary uniform effective magnetic field ($\mathbf{\Omega}_{an}$) acting upon the polariton pseudospins. The orientation of the field is determined by the direction of the anisotropic feature creating it. Despite the fact that such a constant effective magnetic field has been observed in many different samples and experiments,[30–33] a clear explanation of its origin is still not available.

Here we experimentally study the polarization dynamics of exciton polaritons in the presence of such a field and of the Δ_{LT} splitting, and demonstrate the appearance of the anisotropic OSHE. Furthermore, the anisotropic field enhances the spin precession of polaritons moving along directions given by the field orientation. This is used to efficiently generate spin currents at engineered points in the sample, where a localized photonic defect, creating an isolated peak in the polariton potential, is present. Our results are in agreement with a theoretical model based on the spinor Schrödinger equation, which accounts for both the TE-TM splitting and anisotropic splitting.

II. THEORY

Given their long decoherence time,[34] polaritons can be described by a two-component wave function, $\psi_i(\mathbf{k})$, where i represents either spin-up (+) or spin-down (−) polaritons (here we consider only the lower branch). These two spin components are directly coupled to the circular polarizations of external light, allowing for their optical excitation and polarization-resolved detection. The two-dimensional

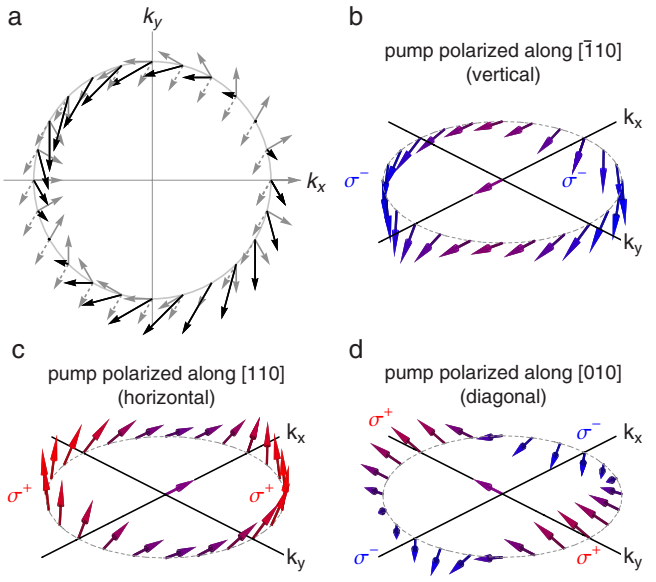

FIG. 2. (Color online) (a) The Δ_{LT} splitting (gray solid arrows) and polarization anisotropy (gray dashed arrows) can be represented by effective magnetic fields, which act on the polariton pseudospin vector (Stokes vector). The total effective magnetic field (black arrows) causes the polariton pseudospin vectors to precess. The Δ_{LT}-related field has been calculated for a pumped pseudospin pointing in the k_x direction. Panels (b)–(d) illustrate the expected evolution of the pseudospin of polaritons that have elastically (Rayleigh) scattered from the pump state (at $k=0$) to a ring in reciprocal space for different planes of linear polarization of excitation. The purple arrow in the center depicts the initial pseudospin. Pseudospins pointing out of the $k_z=0$ plane give rise to circularly polarized emission.

(spinor) wave function obeys a Schrödinger equation, which can be written as[35]

$$i\hbar\frac{\partial\psi_i(\mathbf{k})}{\partial t} = \hat{\mathbf{H}}_{ij}(\mathbf{k})\psi_j(\mathbf{k}) + \int V(\mathbf{k}')\psi_i(\mathbf{k}-\mathbf{k}')d\mathbf{k}' + f_i(\mathbf{k}) - \frac{i\hbar}{2\tau(\mathbf{k})}\psi_i(\mathbf{k}). \quad (1)$$

The Hamiltonian can be written as

$$\hat{\mathbf{H}}_{ij}(\mathbf{k}) = \delta_{ij}T(\mathbf{k}) + \frac{\hbar}{2}[\sigma\cdot\mathbf{\Omega}(\mathbf{k})]_{ij}, \quad (2)$$

where $T(\mathbf{k})$ represents the (nonparabolic) dispersion of lower branch polaritons, σ is the Pauli matrix vector, and $\mathbf{\Omega}$ is an effective magnetic field. $\mathbf{\Omega}$ is given as the sum of a field representing the Δ_{LT} splitting[20] (this field depends on the direction of the polariton wave vector, $\mathbf{k}$) and an effective field arising from the anisotropy in the microcavity heterostructure $\mathbf{\Omega}_{an}$ (this field is wave vector independent). These fields are illustrated in Fig. 2(a). The direction of $\mathbf{\Omega}_{an}$ is chosen to match experimental measurements (see Fig. 4 and the corresponding discussion later).

Here we assume that the TE-TM splitting and the anisotropic splitting have the same value, that is, the associated effective magnetic fields $\mathbf{\Omega}_{an}$ and $\mathbf{\Omega}_{LT}$ have the same mag-

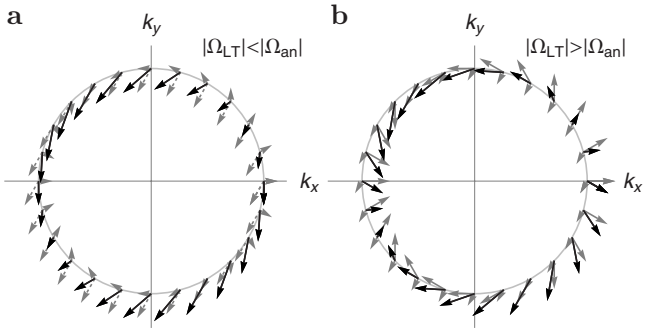

FIG. 3. Although in our experiment $|\mathbf{\Omega}_{LT}| \approx |\mathbf{\Omega}_{an}|$, the situations $|\mathbf{\Omega}_{LT}| < |\mathbf{\Omega}_{an}|$ or $|\mathbf{\Omega}_{LT}| > |\mathbf{\Omega}_{an}|$ could also be realized, for example, by varying the pump energy. The effect of such variation on the total effective magnetic field is shown above; as in Fig. 2(a), the effective magnetic fields caused by Δ_{LT} (gray solid arrows), polarization anisotropy (gray dashed arrows), and the total (black arrows) are illustrated.

nitude. With this condition the theory gives results consistent with the experiment presented here. The situations where $|\mathbf{\Omega}_{LT}| < |\mathbf{\Omega}_{an}|$ or $|\mathbf{\Omega}_{LT}| > |\mathbf{\Omega}_{an}|$ could also be realized under different excitation conditions ($|\mathbf{\Omega}_{LT}|$ depends on the pump energy), resulting in different azimuthal dependences of the total effective field $\mathbf{\Omega}$, as shown in Fig. 3, giving rise to different OSHE patterns as we will see below.

In Eq. (1), $V(\mathbf{k})$ represents the polariton potential. We will consider two kinds of profile: one representing the disorder, which is generated by a stochastic field[36] characterized by a correlation length l and a root-mean-square (rms) amplitude W_{rms} and one representing an isolated peak. The continuous-wave optical pump is described by

$$f_i(\mathbf{k}) = A_i e^{-\mathbf{k}^2 L^2/4} \frac{i\Gamma e^{-iE_p t/\hbar}}{T(\mathbf{k}) - E_p - i\Gamma}, \tag{3}$$

where the pump is Gaussian shaped with energy E_p, linewidth Γ, spot-size L, and amplitude and polarization given by A_i. Unlike the experiments in Refs. 16 and 35 we are working with a pump oriented at normal incidence (which excites polaritons with zero in-plane wave vector, $k=0$). Provided the pump energy is tuned above the energy $T(0)$, Rayleigh scattering still allows the excitation of a ring in reciprocal space [see Fig. 4(a)], which is essential for the observation of the OSHE. Note that Rayleigh scattering alone preserves the polariton polarization.

The decay of polaritons caused by exciton recombination and the escape of photons through the Bragg mirrors of the microcavity is modeled phenomenologically with a lifetime, $\tau(\mathbf{k})$, which can be related to the exciton and photon lifetimes, τ_X and τ_C, respectively, by $1/\tau(\mathbf{k}) = |X(\mathbf{k})|^2/\tau_X + |C(\mathbf{k})|^2/\tau_C$, where $X(\mathbf{k})$ and $C(\mathbf{k})$ are the Hopfield coefficients.[37,38]

The reason for defining the effective magnetic field $\mathbf{\Omega}$ is that it allows a qualitative understanding of the combined effects of TE-TM splitting and anisotropy. The polarization state of polaritons can be represented by the pseudospin vector $\rho = (S_x/S_0, S_y/S_0, S_z/S_0)$, equivalent to the Stokes vector for light, where $S_x = \psi_+^* \psi_- + \psi_-^* \psi_+$, $S_y = i(\psi_-^* \psi_+ - \psi_+^* \psi_-)$, $S_z = |\psi_+|^2 - |\psi_-|^2$, and $S_0 = |\psi_+|^2 + |\psi_-|^2$. Graphically, in the Poincaré sphere, S_x and S_y are the pseudospin coordinates lying on the equatorial plane, which represent the degree and plane of the linearly polarized component of the polarization while S_z describes its circularly polarized component.[16] The field $\mathbf{\Omega}$ causes the pseudospin vector to precess, giving rise to the appearance of circularly polarized emission even under linearly polarized excitation. Figures 2(b)–2(d) illustrate the pseudospin precession for different linear polarizations of the pump. In the experiments presented in the next section we will study the effect of the anisotropic magnetic field on the OSHE patterns via the observation of the degree of circular polarization which arises from the pseudospin precession.

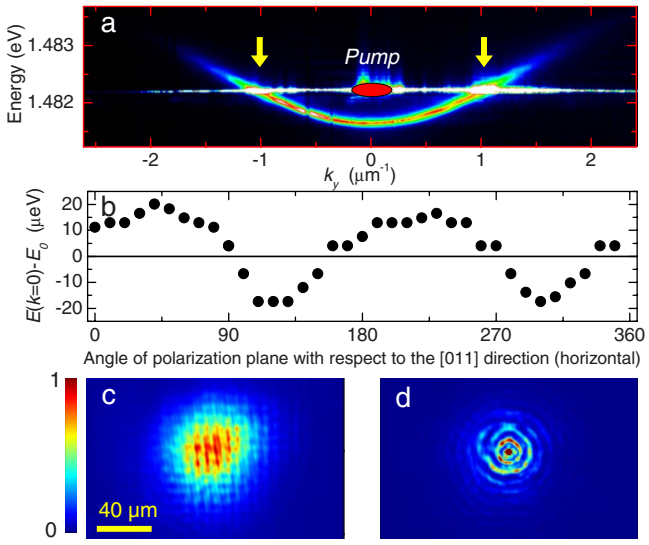

FIG. 4. (Color online) (a) LPB luminescence under out of resonance excitation at $k=0$ (indicated by the red spot). Resonant Rayleigh scattering takes place to LPB states marked by arrows. (b) Energy of the photoluminescence peak at $k=0$ under circularly polarized excitation as a function of the angle of the detected linear-polarization plane ($E_0 = 1.487572$ eV). (c) Real space transmitted intensity in the presence of the shallow disorder usual in standard microcavities and (d) in the presence of a localized photonic defect in the center of the spot. Each panel has been normalized to show the best visibility.

III. EXPERIMENTAL RESULTS

The sample used in our experiments is a 2λ, GaAs/AlAs cavity with one $In_{0.04}Ga_{0.96}As$ quantum well at each of the three antinodes of the confined electromagnetic field, with front/back reflectors with 21/24 pairs.[39] The measured Rabi splitting at low temperature is 5.1 meV. All our experiments were performed at 5 K, at zero exciton-photon detuning, using a linearly polarized single mode laser as the excitation source on a spot of 48 μm in diameter. Real and momentum space images of the emission (circular polarization resolved) were collected in transmission geometry using two high-definition charge-coupled-device (CCD) cameras.

The size and direction of $\mathbf{\Omega}_{an}$ has been obtained by analyzing the linear-polarization-resolved photoluminescence emission of the lower polariton branch (LPB) at $k=0$, where

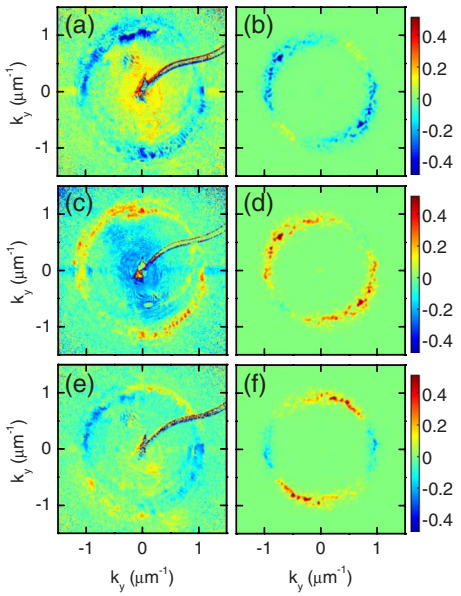

FIG. 5. (Color online) Far-field circular polarization degree detected experimentally (left column) and compared to theory (right column) for the cases of linearly polarized pump excitation along the [(a) and (b)] [$\bar{1}10$] direction—vertical, [(c) and (d)] [110] direction—horizontal, and [(e) and (f)] [010] direction—diagonal. These three cases correspond to Figs. 2(b)–2(d), respectively. Parameters: l=0.2 μm, W_{rms}=0.05 meV, E_p=0.63+T(0) meV, Γ =0.05 meV, L=68 μm, τ_X=100 ps, and τ_C=2 ps. The polarization splitting arising from anisotropy and TE-TM splitting were each assumed equal to 0.04 meV. The shadow in panels (a), (c), and (e) is caused by a block of the pump field to avoid saturation of the detector.

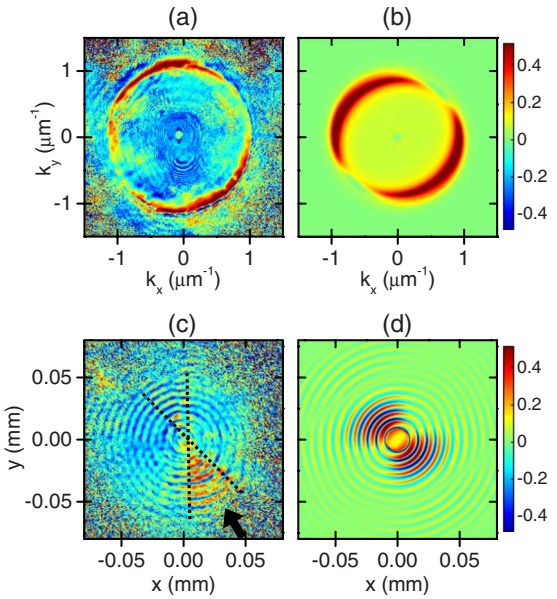

FIG. 6. (Color online) Far-field [near-field] degree of circular polarization detected experimentally (a) [(c)] and compared to theory (b) [(d)] for the case of vertically polarized excitation in the presence of a peak in the polariton potential, in the center of panels (c) and (d). The parameters were the same as in Fig. 5, except that the disorder potential was replaced by a Gaussian shaped defect of height 1 meV and full width at half maximum equal to 3.3 μm. Dotted lines in panel (c) show the region where the spin currents flow, in the direction given by the arrow.

the TE-TM splitting vanishes, as depicted in Fig. 4(b). A splitting due to the anisotropy-related effective field $\mathbf{\Omega}_{an}$ of about 0.04 meV can be observed. The splitting is between linear polarizations oriented at 30° and 120° from the [110] crystallographic direction (k_x, referred to as *horizontal* for convenience) and it is therefore represented by an $\mathbf{\Omega}_{an}$ oriented 60°/240° from the [110] axis, as illustrated in Fig. 2 (for $\mathbf{\Omega}_{an}$ at 240°). The choice between the two possible signs of the field (i.e., pointing either at 60° or 240°) has been unambiguously done to match the orientation of the OSHE patterns discussed below.

We have considered the anisotropic spin Hall effect at two different locations on our sample. At the first location the polariton potential is the typical shallow disordered one present in microcavities, evidenced via the meshed pattern in the real-space image of the transmission intensity [Fig. 4(c)]. In the second location, just 150 μm away from the first one, excitation is performed on top of a photonic defect [Fig. 4(d)]. The presence of the defect results in Airy ringlike patterns which arise from the interference of the k=0 pumped polaritons and those scattered into the Rayleigh ring. The observed fringe separation is of $\Delta l \approx 5.6$ μm which corresponds to the momentum of the scattered polaritons ($k = 2\pi/\Delta l \approx 1.1$ μm^{-1}).

Figure 5 shows, for the first location with shallow disorder [Fig. 4(c)], the measurement of the circular polarization degree (z component of ρ in momentum space for different pump polarizations. The results are quantitatively reproduced by the numerical solutions of Eq. (1).

Under excitation linearly polarized in the plane parallel to the crystallographic directions [$\bar{1}10$] [referred to as *vertical* for convenience; Figs. 5(a) and 5(b)] and [110] [i.e., horizontal; Figs. 5(c) and 5(d)], only two quadrants of circular degree of polarization are visible. This is a direct consequence of the presence of the intrinsic momentum independent effective magnetic field $\mathbf{\Omega}_{an}$, which is canceled by the TE-TM field in the positive diagonal direction ([100]) in the far field [as depicted in Fig. 2(a)]. Polaritons scattered into this diagonal direction do not feel the action of any field and their linearly polarized pseudospin does not precess, not giving rise to any circularly polarized component. On the other hand, the total field is enhanced in the opposite diagonal direction ([010]), giving rise to an increased degree of circular polarization with respect to the case of $\mathbf{\Omega}_{an}$=0.

In the absence of $\mathbf{\Omega}_{an}$, four alternating circular polarization quadrants would be expected as a consequence of the distribution of the TE-TM-related magnetic field in the Rayleigh circle, independently of the polarization plane of the injected polaritons,[16] which is the characteristic signature of the *standard* OSHE. In the presence of $\mathbf{\Omega}_{an}$ we can recover the four quadrants if we rotate the polarization plane of the excitation with respect to the direction of the intrinsic magnetic field so that they are parallel, as shown in Figs. 5(e) and 5(f). For such injected pseudospin the composition of $\mathbf{\Omega}_{an}$ and the TE-TM-related field are canceled at four points in the Rayleigh circle, which delimit the four quadrants [see Fig. 2(d)].

We can take advantage of the enhancement in the spin precession related to the existence of the anisotropic field to observe spin currents. They can be directly generated if excitation is performed at the location where the photonic defect is present [Fig. 4(d)]. Here, under vertically polarized excitation, the anisotropic field gives rise to a distribution of the circular polarization degree in reciprocal space [Figs. 6(a) and 6(b)] similar to that of Figs. 5(a) and 5(b). The presence of the defect results in a strengthening of both the total intensity and the polarization degree of the Rayleigh signal (by a factor of 2.7). The real-space images [Figs. 6(c) and 6(d)] clearly show spin currents of polaritons scattered from the defect in the negative diagonal direction, even without blocking the residual transmitted pump.[40] These spin currents could not be observed in the absence of a defect because in this case scattering takes place homogeneously all over the excitation spot. If we turn by 90° the plane of the polarization of excitation, spin currents follow the same direction with opposite sign (not shown). Note that the concentric ringlike structure of Fig. 4(d) is still observable in the polarization degree, both in the experimental and simulation images.

IV. CONCLUSION

The OSHE relies on the combined effects of Rayleigh scattering of polaritons and pseudospin precession, well described by the introduction of effective magnetic fields physically representing the polarization splitting caused by TE-TM splitting and/or sample anisotropy. The Rayleigh scattering can be engineered to occur at specific points in the microcavity sample, where directional spin currents are efficiently generated and enhanced due to the presence of the intrinsic anisotropic fields. These features can be exploited for the implementation of integrated light-polarization-based logic gates.[17]

ACKNOWLEDGMENTS

We are very grateful to R. Houdré for providing us with the microcavity sample. This work was supported by the IFRAF. A.A. was funded by the Agence Nationale pour la Recherche and A.B. is a member of the Institut Universitaire de France. A.K. acknowledges the support from the EU IRSES projects POLALAS and ROBOCON.

[1] P. M. Tedrow and R. Merservey, Phys. Rev. Lett. **26**, 192 (1971).
[2] M. Julliere, Phys. Lett. A **54**, 225 (1975).
[3] M. Johnson and R. H. Silsbee, Phys. Rev. Lett. **55**, 1790 (1985).
[4] Th. Gerrits, H. A. M. van den Berg, J. Hohlfeld, L. Bär, and Th. Rasing, Nature (London) **418**, 509 (2002).
[5] H. Dery, P. Dalal, Ł. Cywiński, and L. J. Sham, Nature (London) **447**, 573 (2007).
[6] D. D. Awschalom and M. E. Flatté, Nat. Phys. **3**, 153 (2007).
[7] H. J. Zhu, M. Ramsteiner, H. Kostial, M. Wassermeier, H.-P. Schonherr, and K. H. Ploog, Phys. Rev. Lett. **87**, 016601 (2001).
[8] A. T. Hanbicki, B. T. Jonker, G. Itskos, G. Kioseoglou, and A. Petrou, Appl. Phys. Lett. **82**, 4092 (2003).
[9] X. Jiang, R. Wang, R. M. Shelby, R. M. Macfarlane, S. R. Bank, J. S. Harris, and S. S. P. Parkin, Phys. Rev. Lett. **94**, 056601 (2005).
[10] M. I. Dyakonov and V. I. Perel, Phys. Lett. A **35**, 459 (1971).
[11] Y. K. Kato, R. C. Myers, A. C. Gossard, and D. D. Awschalom, Science **306**, 1910 (2004).
[12] J. Wunderlich, B. Kaestner, J. Sinova, and T. Jungwirth, Phys. Rev. Lett. **94**, 047204 (2005).
[13] T. Kimura, Y. Otani, T. Sato, S. Takahashi, and S. Maekawa, Phys. Rev. Lett. **98**, 156601 (2007).
[14] V. Sih, R. C. Myers, Y. K. Kato, W. H. Lau, A. C. Gossard, and D. D. Awschalom, Nat. Phys. **1**, 31 (2005).
[15] J. M. Kikkawa, I. P. Smorchkova, N. Samarth, and D. D. Awschalom, Science **277**, 1284 (1997).
[16] C. Leyder, M. Romanelli, J. Ph. Karr, E. Giacobino, T. C. H. Liew, M. M. Glazov, A. V. Kavokin, G. Malpuech, and A. Bramati, Nat. Phys. **3**, 628 (2007).
[17] T. C. H. Liew, A. V. Kavokin, and I. A. Shelykh, Phys. Rev. Lett. **101**, 016402 (2008).
[18] C. Leyder, T. C. H. Liew, A. V. Kavokin, I. A. Shelykh, M. Romanelli, J. Ph. Karr, E. Giacobino, and A. Bramati, Phys. Rev. Lett. **99**, 196402 (2007).
[19] A. Kavokin, J. J. Baumberg, G. Malpuech, and F. P. Laussy, *Microcavities* (Oxford University Press, New York, 2007).
[20] A. Kavokin, G. Malpuech, and M. Glazov, Phys. Rev. Lett. **95**, 136601 (2005).
[21] M. Z. Maialle, E. A. de Andrada e Silva, and L. J. Sham, Phys. Rev. B **47**, 15776 (1993).
[22] G. Panzarini, L. C. Andreani, A. Armitage, D. Baxter, M. S. Skolnick, V. N. Astratov, J. S. Roberts, A. V. Kavokin, M. R. Vladimirova, and M. A. Kaliteevski, Phys. Rev. B **59**, 5082 (1999).
[23] W. Jantsch and Z. Wiliamowski, in *Spin Physics in Semiconductors*, edited by M. I. Dyakonov (Springer, Berlin, 2007), p. 179.
[24] E. Peter, P. Senellart, D. Martrou, A. Lemaitre, J. Hours, J. M. Gerard, and J. Bloch, Phys. Rev. Lett. **95**, 067401 (2005).
[25] E. A. de Andrada e Silva, G. C. La Rocca, and F. Bassani, Phys. Rev. B **55**, 16293 (1997).
[26] B. Jusserand, D. Richards, H. Peric, and B. Etienne, Phys. Rev. Lett. **69**, 848 (1992).
[27] T. Koga, J. Nitta, T. Akazaki, and H. Takayanagi, Phys. Rev. Lett. **89**, 046801 (2002).
[28] M. M. Glazov, I. A. Shelykh, G. Malpuech, F. Laussy, K. V. Kavokin, and A. V. Kavokin, Phys. Status Solidi C **4**, 638 (2007).
[29] W. Langbein, V. Savona, D. Reuter, and A. D. Wieck, in Tenth International Conference on the Optics of Excitons in Confined Systems, Patti, Italy, 2007 (unpublished).
[30] Ł. Kłopotowski, M. D. Martín, A. Amo, L. Viña, I. A. Shelykh, M. M. Glazov, G. Malpuech, A. V. Kavokin, and R. André, Solid State Commun. **139**, 511 (2006).
[31] D. N. Krizhanovskii, D. Sanvitto, I. A. Shelykh, M. M. Glazov,

G. Malpuech, D. D. Solnyshkov, A. Kavokin, S. Ceccarelli, M. S. Skolnick, and J. S. Roberts, Phys. Rev. B **73**, 073303 (2006).
[32] J. Kasprzak, M. Richard, S. Kundermann, A. Baas, P. Jeambrun, J. M. J. Keeling, F. M. Marchetti, M. H. Szymanska, R. Andre, J. L. Staehli, V. Savona, P. B. Littlewood, B. Deveaud, and L. S. Dang, Nature (London) **443**, 409 (2006).
[33] G. Roumpos, C.-W. Lai, T. C. H. Liew, Y. G. Rubo, A. V. Kavokin, and Y. Yamamoto, Phys. Rev. B **79**, 195310 (2009).
[34] W. Langbein, I. Shelykh, D. Solnyshkov, G. Malpuech, Y. Rubo, and A. Kavokin, Phys. Rev. B **75**, 075323 (2007).
[35] T. C. H. Liew, C. Leyder, A. V. Kavokin, A. Amo, J. Lefrere, E. Giacobino, and A. Bramati, Phys. Rev. B **79**, 125314 (2009).
[36] V. Savona and W. Langbein, Phys. Rev. B **74**, 075311 (2006).
[37] H. Haug and S. W. Koch, *Quantum Theory of the Optical and Electronic Properties of Semiconductors* (World Scientific, Singapore, 1994).
[38] F. P. Laussy, G. Malpuech, A. V. Kavokin, and P. Bigenwald, J. Phys.: Condens. Matter **16**, S3665 (2004).
[39] R. Houdré, C. Weisbuch, R. P. Stanley, U. Oesterle, and M. Ilegems, Phys. Rev. B **61**, R13333 (2000).
[40] In Ref. 16, the observation of the spin currents in real space was only possible when blocking the residual transmitted pump in the far field, before forming the real-space image in the CCD.